JOURNAL OF GEOPHYSICAL RESEARCH, VOL. 106, NO. D3, PAGES 3095–3110, FEBRUARY 16, 2001

Total VOC reactivity in the planetary boundary layer 2. A new indicator for determining the sensitivity of the ozone production to VOC and NO_x

Frank Kirchner, Francois Jeanneret, Alain Clappier, Bernd Krüger, Hubert van den Bergh, and Bertrand Calpini

Air Pollution Laboratory, Swiss Federal Institute of Technology, Lausanne, Switzerland

Abstract. A new indicator is proposed for determining if tropospheric ozone production in a specific area is limited by VOC or NO_x. The indicator $\Theta = \tau_{OH}^{VOC}/\tau_{OH}^{NO_x}$ describes the ratio of the lifetimes of OH against the losses by reacting with VOC and NO_x. Whereas $\tau_{OH}^{NO_x}$ can be obtained by conventional measurements, the new pump and probe OH approach which is described in part one of this publication makes it now possible to obtain also τ_{OH}^{VOC}. Indicator values above a threshold value of 0.2 ± 50% are representative of NO_x-saturated conditions where an increase of NO_x emissions causes lower ozone production. For values below 0.01 the ozone production is very insensitive to changes of VOC emissions. The robustness of this indicator against several parameters such as temperature, humidity, photolysis, and initial ozone concentrations is tested in a box model and compared to the robustness of other earlier proposed indicators. In contrast to earlier proposed indicators, this new one is not based on photochemically produced long-lived species but describes the instantaneous regime of an air parcel. Three-dimensional simulation shows that this indicator is quite successful in estimating the impact of increased or reduced emissions on the ozone concentrations for each location in the modeling area. This will make it a very helpful tool for developing ozone abatement strategies.

1. Introduction

High tropospheric ozone concentrations are currently a problem in many parts of the world. To develop effective abatement strategies, it is necessary to know whether in a specific area the ozone production is limited by the emission of volatile organic compounds (VOC), by the emission of NO_x, or by both of them (regimes I, III, and II in Figure 1, respectively). This limitation can change from one location to another and within one location with the time.

Several possibilities exist to determine whether VOC or NO_x is the limiting factor for the ozone production. One way is to perform three-dimensional model calculations with several scenarios by increasing and decreasing the VOC and NO_x concentrations to evaluate the changes in the simulated ozone concentrations. In situ measurements may bring complementary and important information. It is thus necessary to find parameters which can easily be measured in situ on the one hand and which indicate the regime of ozone formation. Important for an indicator is its sensitivity to the parameter of interest and its insensitivity to all other parameters. Several indicators have been proposed, for example, the afternoon concentrations of NO_y [*Milford et al.*, 1994], O_3/NO_z (with $NO_z = NO_y - NO_x$), and H_2O_2/HNO_3 [*Sillman*, 1995]. Common to all these indicators is that they are based on photochemically produced, relatively long-lived species and therefore act like an integral over the past of the investigated air parcel. This makes it somewhat difficult to attribute a regime to the place of emission as is necessary for the development of abatement strategies. In addition, the concentrations of species such as H_2O_2 and NO_z are considerably influenced by dry deposition, which is regarded as the major source of uncertainties in model calculations of these species [*Sillman et al.*, 1998]. According to a study of *Lu and Chang* [1998], the threshold values of these indicators may vary for different locations.

In this work, a new indicator is proposed which provides the sensitivity of the potential ozone formation to changes in the concentrations of VOC and NO_x at the place and the time of the emission: $\Theta = \tau_{OH}^{VOC}/\tau_{OH}^{NO_x}$, where τ_{OH}^{VOC} is the lifetime of OH against the loss by reaction with VOC and $\tau_{OH}^{NO_x}$ is the lifetime of OH against the loss by reaction with NO_x. This indicator can easily be measured by combining standard methods and the new pump and probe method which is described by *Calpini et al.* [1999] and *Jeanneret et al.* [this issue]. In this pump and probe approach, high amounts of OH radicals are produced by laser photolysis of the ambient ozone in the presence of water vapor, and the OH decay is followed by laser-induced fluorescence spectroscopy. As this value Θ may also easily be obtained from model calculations, this indicator can be a helpful tool for the interpretation of field measurements as well as of modeling results and can support the development of ozone abatement strategies.

2. Sensitivity of the Ozone Production to VOC and NO_x

Three regimes of ozone production are distinguished in Figure 1. This figure results from a box model study where the ozone production from different VOC and NO_x concentra-

Paper number 2000JD900603.
0148-0227/01/2000JD900603$09.00

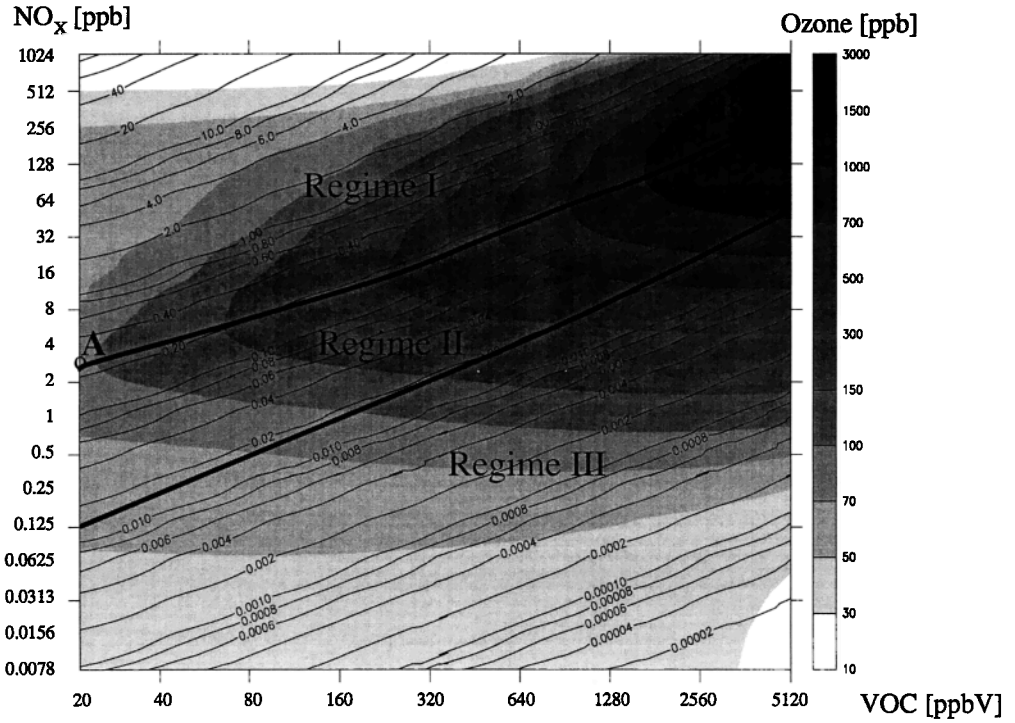

Figure 1. Plot of the ozone mixing ratios against the NO_x and VOC mixing ratios from the box model runs for the base case N4 defined in Table 2. The bold lines are the borders of the three regimes of ozone formation, and the thin lines represent the values of the indicator $\Theta = \tau_{OH}^{VOC}/\tau_{OH}^{NO_x}$ calculated with RACM mechanism.

tions was calculated. This figure will be discussed in detail later. In regime I, increasing NO_x decreases ozone. In regime III the ozone formation is nearly insensitive to changes in the VOC. In regime II the changes in the ozone concentrations are positively correlated to the changes in the concentrations of VOC and NO_x.

Figure 2 gives an overview of the most important reactions connected to the ozone formation. In this picture the numbers in brackets correspond to the equation numbers in the text. Essential for the ozone formation is the cycle of odd hydrogen (odd H) which can be defined as the sum of OH, HO_2, and RO_2 [*Kleinman*, 1986, 1991]:

(R1) $\quad OH + VOC[+O_2] \rightarrow RO_2 + H_2O$

(R2) $\quad RO_2 + NO[+O_2]$

$$\rightarrow (HO_2 \text{ or } R'O_2) + NO_2 + \text{oxygenated VOC}.$$

HO_2 is formed if the intermediately formed alkoxy radical RO reacts with O_2. $R'O_2$ is formed if RO reacts by isomerization or decomposition. In most cases the R'O resulting from the reaction of $R'O_2$ with NO will produce HO_2. In Figure 2 the formation of $R'O_2$ is neglected.

(R3) $\quad HO_2 + NO \rightarrow OH + NO_2.$

Because (R2) and (R3) of this cycle convert NO to NO_2, this cycle drives the ozone production.

(R4) $\quad NO_2 + h\nu \rightarrow NO + O(^3P)$

(R5) $\quad O(^3P) + O_2 \rightarrow O_3.$

The amount of odd hydrogen can be increased by the reactions of VOC with other reactive radicals such as NO_3 or O_3 or by photolysis reactions, for example:

(R6) $\quad O_3 + h\nu \rightarrow O(^1D) + O_2$

(R7) $\quad O(^1D) + H_2O \rightarrow 2OH.$

It is decreased if odd hydrogen radicals react with each other:

(R8) $\quad RO_2 + R'CH_2O_2 \rightarrow \gamma(ROH + R'CHO)$

$$+ (1 - \gamma)(RO + R'CH_2O) + O_2$$

(R9) $\quad HO_2 + HO_2 \rightarrow H_2O_2 + O_2$

(R10) $\quad RO_2 + HO_2 \rightarrow ROOH + O_2$

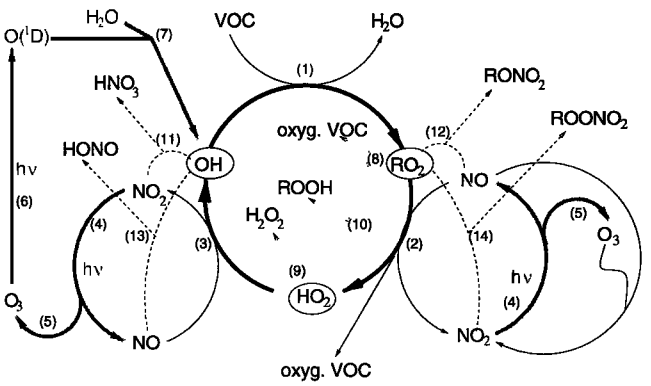

Figure 2. Important reactions for the ozone formation. The bold arrows represent the odd hydrogen cycle. The gray arrows represent radiation-dependent reactions. The numbers in brackets correspond to the equation numbers in the text.

and if reactions of odd hydrogen with NO_x provide stable products:

(R11) $OH + NO_2[+M] \rightarrow HNO_3[+M]$

(R12) $RO_2 + NO[+M] \rightarrow RONO_2[+M]$

(R13) $OH + NO[+M] \rightarrow HONO[+M]$

(R14) $RO_2 + NO_2[+M] \rightarrow ROONO_2[+M]$.

The odd H loss via (R13) and (R14) is only temporary because of the inverse reactions

(-R13) $HONO + h\nu \rightarrow OH + NO$

(-R14) $ROONO_2 \rightarrow RO_2 + NO_2$.

Under NO_x-saturated conditions (regime I in Figure 1, often called "VOC-controlled") the NO_x concentrations are high, and the loss of odd H by (odd H + odd H) self-reactions is low because HO_2 and RO_2 radicals react nearly completely with NO or NO_2. Because the rates of the reactions of NO with HO_2 and RO_2 are limited by the peroxy radical concentrations, an increase of the NO_x concentrations cannot increase the NO to NO_2 conversion speed and therefore cannot increase the ozone production. On the other hand, increased NO_x levels lead to an increased loss of odd H by the (OH + NO_2) reaction. Because VOCs compete with NO_2 for OH, an increase in the VOC concentrations lowers the odd H loss from the (OH + NO_2) reaction and increases the RO_2 production. Hence an increase of VOC leads to enhanced ozone values, whereas an increase of NO_x lowers the ozone concentration. The border between regime I and regime II is characterized by the highest possible ozone production for a given VOC concentration. This is visualized in Figure 3a that is a section of Figure 1 keeping VOC constant equal to 80 ppbv. Varying the NO_x mixing ratios for a constant VOC concentration leads to an ozone maximum which separates regime I from regime II. The indicator $\Theta = \tau_{OH}^{VOC}/\tau_{OH}^{NO_x}$ represents the relationship of the competing reactions (NO_x + OH) and (VOC + OH) and is therefore able to distinguish between regimes I and II.

In the regime of pure NO_x control (regime III in Figure 1) the NO_x concentrations are low, and the reaction (odd H + odd H) becomes an important odd H loss reaction. The limiting parameter for the NO to NO_2 conversion is no longer the amount of HO_2 or RO_2 but the amount of available NO. Therefore an increase of NO_x enhances the NO to NO_2 conversion and the ozone production. In contrast, an increase of the VOC concentrations only accelerates the OH to RO_2 conversion, but because RO_2 is not the limiting factor for the NO to NO_2 conversion, it cannot increase the ozone production. The border between regime II and regime III is not defined by the highest possible ozone production for a given NO_x concentration but by a line at which the increase in the ozone concentrations caused by adding VOC becomes very small. This is visualized in Figure 3b which is a section of Figure 1 keeping NO_x constant equal to 2 ppb and will be discussed later in detail (see equation (1) in section 3 below and associated discussion). Note that the VOC axis has a logarithmic scale. The relationship of RO_2 and NO is crucial in determining how much RO_2 drives the NO_x cycle and how much is removed by (odd H + odd H) reactions. NO concentration is linked to the NO_x concentration and therefore to the lifetime $\tau_{OH}^{NO_x}$. The amount of produced RO_2 radicals is linked to the rate $k_{OH}^{VOC}.C_{VOC}$ where C_{VOC} is the concentration of VOC. Therefore it is linked to the lifetime τ_{OH}^{VOC}. Thus the indicator $\Theta = \tau_{OH}^{VOC}/\tau_{OH}^{NO_x}$ is also expected to be able to distinguish between regimes II and III.

3. Test of the Indicator $\Theta = \tau_{OH}^{VOC}/\tau_{OH}^{NO_x}$ in a Box Model Study

The first tests of the indicator Θ were performed with a box model. With box model runs one may investigate the sensitivity of the indicator to a large number of different parameters keeping the concentrations in each run so stable that the regime can be kept unchanged during the run. In this way it is possible to determine the robustness of that indicator. It will be compared to the robustness of the other proposed indicators NO_y, O_3/NO_z, and H_2O_2/HNO_3. The model conditions are summarized in Table 1. The applied mechanism was the RACM mechanism [*Stockwell et al.*, 1997] which is a further development of the older RADM 2 mechanism [*Stockwell et al.*, 1990].

Table 2 shows the calculated scenarios and the resulting indicator values. The simulations were done in two steps. For each scenario, 162 box model runs (started at 0600 LT and stopped at 1500 LT of the same day) were performed varying the VOC mixing ratios in nine steps between 20 ppbv and 5 ppmv (20, 40, 80, 160, 320, 640, 1280, 2560, 5120 ppbv) and the NO_x mixing ratios in 18 steps between 8 ppt and 1 ppm (0.0078, 0.0156, 0.03125, 0.0625, 0.125, 0.25, 0.5, 1, 2, 4, 8, 16, 32, 64, 128, 256, 512, 1024 ppb). To define the border between regimes I and II more precisely, in a second step close to the preliminary determined border the NO_x mixing ratios are varied by 10 times smaller intervals (e.g., between 4 and 8 ppb by 0.4 ppb steps, compare Figure 3a). Thus, for each scenario, 324 box model runs were performed. In both steps the concentrations of NO_x and the nonoxidized VOC were kept constant, corresponding to a situation where the emissions compensate the losses. Oxidized VOC like aldehydes and ketones are formed and degraded in the system; nevertheless, the sum of all VOC is nearly constant during the run. With very few exceptions the increase in the VOC concentrations due to produced oxygenated VOCs is below 20%, and the increase of the VOC reactivity is below 30%.

This constancy of the concentrations is important because it avoids a change of the regime during the run. If the regime would change, for example, at 1400 LT from II to I the ozone formation which was mainly caused by the conditions of regime II would be attributed to regime I, and consequently the determined indicator value would be interpreted incorrectly. A second reason is that a comparison between an indicator like Θ which describe the instantaneous regime and indicators which act like an integral over the past of the investigated air parcel would be much more difficult if the regime has changed during the run.

The VOC split for the base case (N4 in Table 2) was derived by running a box model for 2 days with emissions typical for continental European air ("PLUME2" case in the mechanism comparison of *Kuhn et al.* [1998]). The split calculated for the noon of the second day was modified. The HCHO was reduced from the calculated value of 20% of the total emitted VOC to the more common value of 6% (compare, for example, values given by *Finlayson-Pitts and Pitts* [1986]). This HCHO reduction was compensated for by increasing the nonoxidized VOC species accordingly.

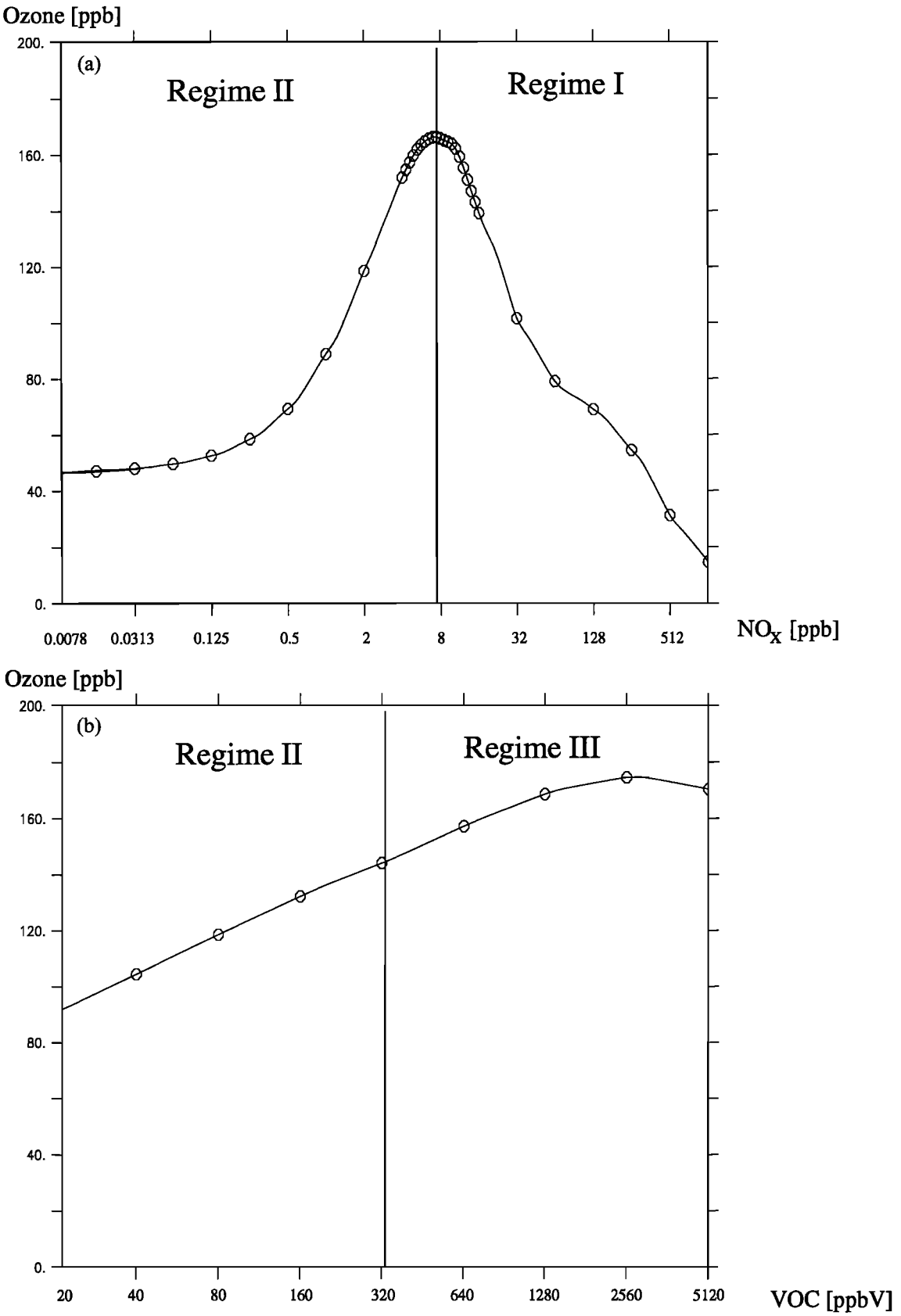

Figure 3. Plot of the ozone concentration calculated for the base case N4 (see Table 2) of the box model runs. The ozone is plotted (a) against NO_x in logarithmic scale keeping VOC constant equal to 80 ppbv and (b) against VOC in logarithmic scale keeping NO_x constant equal to 2 ppb.

Table 1. Conditions for RACM Box Model Calculations[a]

	N, Normal Reactive	R, High Reactive	E, Low Reactive	H, High Nitrate	L, Low Nitrate
Mean k_{VOC}^{OH}, $cm^3\ s^{-1}$	4.1×10^{-12}	7.7×10^{-12}	2.6×10^{-13}	1.1×10^{-11}	3.8×10^{-12}
Methane, ppb	1700	1700	1700	1700	1700
CO, ppb	100	100	100	100	100
O_3, ppb	50 (10–150)	50–100	50–100	50–100	50–100
NO_x	NO_x	NO_x	NO_x	NO_x	NO_x
Ethane	0.053 × VOC	0.032 × VOC	1.000 × VOC	···	0.059 × VOC
Less reactive alkanes HC3	0.429 × VOC	0.260 × VOC	···	···	0.472 × VOC
Medium-reactive alkanes HC5	0.088 × VOC	0.088 × VOC	···	···	···
High-reactive alkanes HC8	0.025 × VOC	0.025 × VOC	···	1.000 × VOC	···
Ethene	0.030 × VOC	0.030 × VOC	···	···	0.034 × VOC
Terminal alkenes OLT	0.0016 × VOC	0.016 × VOC	···	···	0.0016 × VOC
Internal alkenes OLI	0.0004 × VOC	0.004 × VOC	···	···	0.0004 × VOC
Toluene	0.056 × VOC	0.056 × VOC	···	···	0.062 × VOC
Xylene	0.008 × VOC	0.080 × VOC	···	···	0.009 × VOC
HCHO	0.060 × VOC	0.100 × VOC	···	···	0.067 × VOC
Higher aldehydes	0.050 × VOC	0.120 × VOC	···	···	0.056 × VOC
Ketones	0.199 × VOC	0.189 × VOC	···	···	0.239 × VOC
Σ VOC	1.000 × VOC	1.000 × VOC	1.000 × VOC	1.000 × VOC	1.000 × VOC

[a]VOC (ppbv): 20, 40, 80, 160, 320, 640, 1280, 2560, 5120. NO_x (ppb): 0.0078, 0.0156, 0.03125, 0.0625, 0.125, 0.25, 0.5, 1, 2, 4, 8, 16, 32, 64, 128, 256, 512, 1024. Simulation time: 9 hours (0600–1500 LT).

The base case is calculated using the diurnal varying solar radiation of June 21 at 40° north and clear sky and constant values for temperature (298 K) and humidity (0.01 atm water partial pressure). The calculated ozone and indicator values at 1500 LT of the base case N4 are shown in Figure 1. The scale of the axis corresponds to the NO_x and VOC concentrations used in the 162 scenarios. The first step to evaluate the results is to identify the three regimes in each data set from the results at 1500 LT.

3.1. Border Between Regime I and Regime II

The border between regime I and regime II is defined by the highest ozone values found for each VOC mixing ratio. The indicator values belonging to the different regimes were determined by the following procedure. First, for each VOC concentration the ozone maximum resulting by varying the NO_x concentrations is determined. This is visualized in Figure 3a which shows a plot of the ozone mixing ratios against the NO_x

Table 2. Criteria for Determining the Regime (VOC or NO_x Limitation)[a]

					$\tau_{OH}^{VOC}/\tau_{OH}^{NO_x}$				NO_y		O_3/NO_z		H_2O_2/HNO_3			
			Photo-lysis	Initial	I	II	II	III	I	II	I	II	I	II	II	III
Case	T, K	p_{H_2O}, atm	(40°N), day	O_3, ppb	Lowest	Highest	Lowest	Highest	Lowest	Highest	Highest	Lowest	Highest	Lowest	Highest	Lowest
N1	298	0.01	June 21	10	0.14	0.19	0.007	0.027	10	2980	10	0.9	0.075	0.053	23	0.67
N2	298	0.01	June 21	20	0.14	0.21	0.008	0.027	11	3040	11	0.8	0.082	0.047	16	0.67
N3	298	0.01	June 21	30	0.14	0.21	0.008	0.027	11	2990	11	0.9	0.066	0.053	13	0.67
N4	298	0.01	June 21	50	0.14	0.21	0.015	0.027	11	2990	12	0.9	0.079	0.053	7	0.67
N5	298	0.01	June 21	100	0.14	0.27	0.015	0.027	15	3000	13	0.9	0.070	0.053	5	0.66
N6	298	0.01	June 21	150	0.15	0.33	0.008	0.027	19	2990	13	0.9	0.060	0.052	7	0.65
N7	283	0.01	June 21	50	0.08	0.23	0.009	0.016	12	1860	10	1.1	0.103	0.055	7	1.6
N8	283	0.01	June 21	100	0.08	0.25	0.016	0.016	15	1790	11	1.1	0.120	0.057	5	1.6
N9	298	0.005	June 21	50	0.13	0.22	0.015	0.027	10	2860	14	0.9	0.063	0.046	6	0.57
N10	298	0.005	June 21	100	0.13	0.26	0.016	0.028	11	2870	17	0.9	0.058	0.050	4	0.56
N11	298	0.02	June 21	50	0.15	0.27	0.015	0.027	18	3160	8	0.8	0.086	0.062	8	0.85
N12	298	0.02	June 21	100	0.15	0.34	0.015	0.028	24	3160	8	0.8	0.078	0.061	6	0.84
N13	298	0.01	Dec. 21	50	0.10	0.17	0.031	0.029	28	950	52	1.3	0.078	0.060	1.3	0.51
N14	298	0.01	Dec. 21	100	0.10	0.19	0.031	0.032	28	1020	25	1.3	0.086	0.053	0.9	0.50
R1	298	0.01	June 21	50	0.08	0.21	0.015	0.054	29	27400	8	0.1	0.078	0.054	7	0.10
R2	298	0.01	June 21	100	0.08	0.26	0.026	0.055	35	28200	8	0.1	0.066	0.049	3	0.10
E1	298	0.01	June 21	50	0.05	0.39	0.001	0.012	5	26	17	14	0.144	0.091	0.2	0.08
E2	298	0.01	June 21	100	0.07	0.47	0.001	0.021	8	35	19	13	0.115	0.099	0.1	0.004
H1	298	0.01	June 21	50	0.01	0.11	0.082	0.376	9	58	15	14	0.039	0.006	0.03	0.00004
H2	298	0.01	June 21	100	0.01	0.16	0.088	0.778	14	5	15	14	0.045	0.025	0.07	0.00001
L1	298	0.01	June 21	50	0.12	0.15	0.016	0.030	3	950	44	1.2	0.070	0.065	74	0.68
L2	298	0.01	June 21	100	0.11	0.16	0.017	0.031	4	20	68	13	0.113	0.069	56	0.67

[a]Cases: N, normal reactive VOC split; R, more reactive VOC split; E, all VOC equal ethane; H, high nitrate formation, all VOC are large alkanes (HC8 in RACM); L, VOC split with low nitrate formation (see Table 1). After attributing each of the 324 box model runs of one case to the calculated regime, the lowest and/or highest indicator values found for each regime are listed. The definitions for the regimes are the same for all indicators and are explained in the text. The border between regime II and regime III is determined using $\alpha_{lim} = 0.05$ (see text).

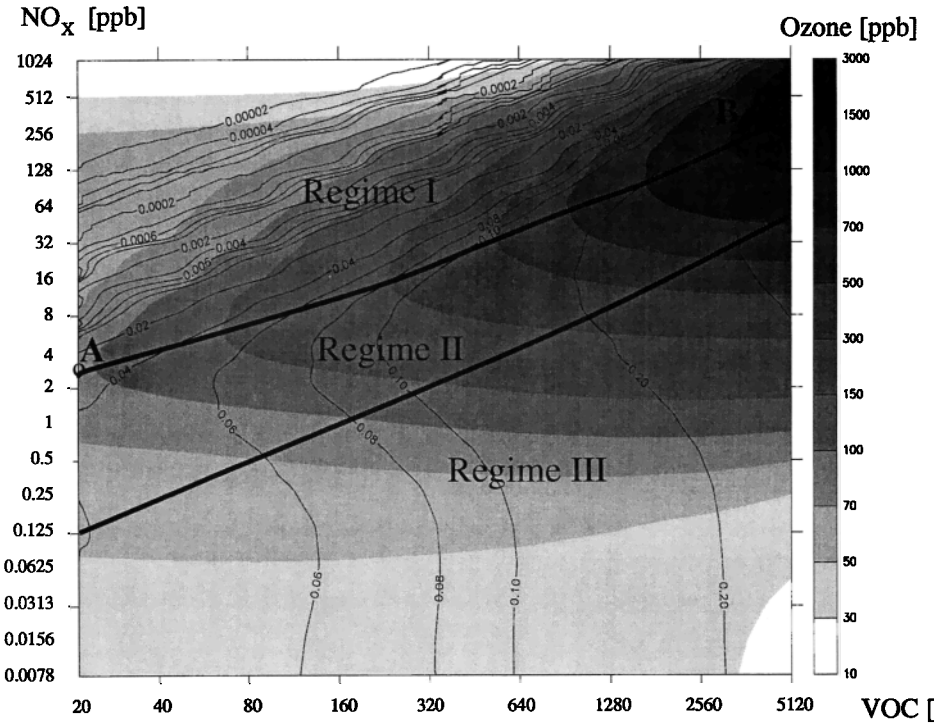

Figure 4. Dependence of the mixing ratios of (RO_2 + HO_2) (in ppb, thin lines) on the mixing ratios of NO_x, VOC, and O_3 resulting from the box model runs of the base case N4. The bold lines are the borders of the three regimes.

mixing ratios keeping VOC constant equal to 80 ppb. Each box model run is symbolized by a circle. The box model runs that are located to the right of the maximum are attributed to regime I; the other ones are attributed to regime II (or III, see below). This is done for all nine different VOC initial concentrations of the case N4. The minimum indicator value of the complete set of all box model runs which are attributed to regime I is determined. In the same way the maximum indicator value of all box model runs which are attributed to regime II is determined. Both values are listed in Table 2.

For N4 the lowest value found for regime I is about 30% lower than the highest value found for regime II. Considering the fact that the indicator values in Figure 1 cover 6 orders of magnitude, this 30% overlap is relatively small; therefore the isolines of the Θ values are nearly parallel to the border between regimes I and II. Being parallel is an important prerequisite required for a good indicator. However, there is a small difference in the slope of the Θ isolines and the regime border which leads to the overlap of regimes I and II found in Table 2. This overlap occurs because the Θ values at the border tend to become smaller for higher VOC concentrations. This trend can be explained in the following way: In Figure 1, point A (describing the ratio 20 ppbv VOC/3 ppb NO_x) is located at the border between regime I and regime II. Increasing the mixing ratios of both VOC and NO_x by 2 orders of magnitude provides the point B (2 ppmv VOC/300 ppb NO_x) which is connected to the same indicator value Θ (because the VOC split remains constant). This point is no longer located at the border but inside regime I. This is because the corresponding concentrations of odd hydrogen are only increased from 30 to 200 ppt and therefore only by 1 order of magnitude as can be seen in Figure 4 where the isolines of the sum of RO_2 and HO_2 are plotted against the VOC, NO_x, and O_3 values of the base case N4. Thus, for the conditions of point B, the ratio (RO_2 + HO_2)/NO_x is smaller than at point A, and the cycle

$$\text{(R2), (R3)} \quad RO_2 \text{ (or } HO_2\text{)} + NO \rightarrow NO_2 + \text{other products}$$

$$\text{(R4)} \quad NO_2 + h\nu \rightarrow NO + O(^3P)$$

is more sensitive to changes in the RO_2 (and therefore in the VOC) concentrations and less sensitive to changes in the NO_x concentrations than at point A. For that reason, increasing the concentrations of both NO_x and VOC without changing the ratio VOC/NO_x (which means in the case of a constant VOC split: without changing the value of Θ) increases the sensitivity to VOC and lowers the sensitivity to NO_x. Hence the border between the regimes is shifted to lower Θ values. However, this shift is not very pronounced, changing the indicator value at the border between regime I and regime II from 0.21 for low NO_x and VOC to 0.14 for high NO_x and VOC (Table 2).

To investigate the robustness of the indicator, several scenarios were calculated using different meteorological conditions, different initial ozone concentrations, and different VOC splits. From the base case N4 the initial ozone concentration was changed (scenarios N1–N6). The temperature was lowered to 283 K (N7 and N8). The humidity was changed by a factor of 2 (N9–N12). The solar radiation was lowered to that of December 21 at 40°N (N13 and N14). The VOC split was varied by replacing all VOC by the low-reactivity ethane (E1 and E2), by large alkanes which produce the highest amounts of nitrates (H1 and H2), by a VOC split which produces very low amount of nitrates (L1 and L2), or by a high-reactivity VOC split which was derived by increasing the most reactive VOC ($k_{VOC}^{OH} > 2 \times 10^{-11}$ cm^3 s^{-1}) by a factor of 10 and lowering the least reactive ones ($k_{VOC}^{OH} \leq 2 \times 10^{-12}$ cm^3 s^{-1}) by 40% (R1 and R2). All these cases were evaluated in the

same way as described for the base case N4. The results are collected in Table 2. The indicator Θ would distinguish perfectly between regimes I and II if the lowest value found in all cases for regime I were larger than the highest value of all cases found for regime II. If that would be the case the indicator would be extremely insensitive to all investigated parameters (e.g., photolysis, humidity, VOC reactivity, etc.) but sensitive to the regime.

The indicator values at the border (lowest values for regime I and highest values for regime II) are slightly positively correlated to the initial O_3 concentrations (N1–N6), photolysis rates (N13, N14), and humidity (N9–N12). This is due to the fact that higher ozone or water concentrations or a higher photolysis rate lead to a higher OH production rate via $O(^1D)$ and therefore compensate higher OH losses caused by the ($OH + NO_2$) reactions. This effect is small. By increasing the reactivity of VOC (scenario R1 and R2) more VOC react in one time step. This is comparable to a higher VOC concentration of a less reactive VOC split like that of the scenarios N1–N6. Hence the indicator values for the highest VOC concentrations are somewhat lower than for the scenarios N1–N6 following the same trend which was discussed before. The highest values found for regime II which are found for relatively low VOC concentrations do not differ from the values found for N1–N6. Decreasing the reactivity of the VOC split drastically (E1 and E2) leads to an increase in the highest values of regime II which is expected for the same reasons. The decrease in the lowest values of regime I is due to the fact that the ozone production in the cases E1 and E2 is very low. Therefore the OH production rate via $O(^1D)$ is small, and the OH losses caused by the ($OH + NO_2$) reactions are much less compensated by OH production than in N4.

The lowest values for regime I are found in scenarios H1 and H2 where the nitrate formation rate of the VOC is artificially high. Twenty-six percent of the produced RO_2 does not participate in the ozone formation but forms nitrate. Hence they also do not produce HO_2 which means a further reduction of the amount of peroxy radicals. As explained before, lowering the amount of active peroxy radicals without lowering the amounts of VOC and NO_x leads to a lower indicator value. This sensitivity to the nitrate formation rate becomes only important for very high nitrate yields. It is not important for moderate nitrate yields. This can be seen comparing the scenarios L1 and L2 where the nitrate formation rate is drastically lowered compared to the corresponding scenarios N4 and N5 with normal nitrate formation: only small changes in the indicator values are found. Combining all box model results, the border between regime I and regime II is given by indicator values of $\Theta = 0.2 \pm 50\%$. Because the largest deviations from 0.2 are found for the most extreme (or the less probable) emission cases, the uncertainty in Θ will be considerably smaller than 50% for most of the application cases.

After submitting our paper, *Tonnesen and Dennis* [2000a] published that the border between regime I and regime II (called "[O_3] ridgeline" in their paper) is associated with an almost constant percentage of OH reacting with VOC of 82–86%. Taking the average value of 84% and estimating that the remaining 16% OH reacts completely with NO_x leads to a value of 0.19 for Θ which agrees very well with our value of 0.2.

3.2. Border Between Regime II and Regime III

Comparing Figure 3b to Figure 3a makes it obvious that the border between regime II and regime III is much more difficult to determine than the border between regimes I and II. In cases where the percentage of alkenes in the VOC split was low there was no maximum at all. However, even in cases where a maximum exists, it is not of practical importance because close to this maximum the changes in the ozone production are very small compared to the changes in the VOC concentrations. Therefore it is necessary to define an arbitrary border between regime II and regime III. Its definition is based on the effect of increased VOC on the ozone production.

$$\alpha = \frac{C_{O_3}(C_{VOC,2}) - C_{O_3}(C_{VOC,1})}{(k^{OH}_{VOCsplit}/k^{OH}_{ref})(C_{VOC,2} - C_{VOC,1})}. \quad (1)$$

The term α is a ratio that expresses the changes in ozone due to changes in VOC: If the VOC concentration is changed from $C_{VOC,1}$ to $C_{VOC,2}$, the ozone concentration changes from $C_{O_3}(C_{VOC,1})$ to $C_{O_3}(C_{VOC,2})$. Because the change in ozone depends on the reactivity of the VOC, this effect is taken into consideration by using the ratio of the mean $k^{OH}_{VOCsplit}$ rate constant of the actual VOC split divided by the mean k^{OH}_{ref} rate constant of a reference VOC split. If additional VOC does not enhance the ozone values, or if the increase in ozone is small enough that α becomes smaller than a threshold value α_{lim}, the corresponding indicator values are attributed to regime III. The values in Table 2 are calculated by using $\alpha_{lim} = 0.05$ using the average rate constant of the base case VOC split as k^{OH}_{ref} (4×10^{-12} cm^3 s^{-1}). Therefore those cases are attributed to regime III where an increase of the average VOC concentration by 20 ppbv VOC (with the average OH reaction rate of 4×10^{-12} cm^3 s^{-1}) leads to less than 1 ppb increase in the ozone.

The variation of the highest values of regime III, calculated using $\alpha_{lim} = 0.05$, is small for most of the cases in Table 2, with a variety of different initial ozone, humidity, temperature, and solar radiation conditions. By changing drastically the VOC split the variation of the highest values of regime III increases. It is only in the case of very high nitrate formation (H1 and H2) that it increases more than a factor of 2. As the VOC mixing ratios are varied by a factor of 2 in the successive box model runs, the precision of the determined values is limited to this factor of 2. Within one data set the overlap of the indicator values of regimes II and III is somewhat more pronounced than for the border between regimes I and II. On the basis of this data an indicator value between 0.01 and 0.03 can be proposed for the border between regimes II and III. However, lowering the α_{lim} value by 1 order of magnitude also lowers the indicator value at that border by 1 order of magnitude. Also increasing α_{lim} by a factor of 4 leads to an increase of the border value of Θ by about the same factor. Hence the value for Θ is highly dependent on the value of α_{lim}. In the base case N4, for α_{lim} values between 0.2 and 0.005, Θ is found to be proportional to α_{lim}.

4. Comparison to Other Indicators

In this chapter the results obtained using Θ are compared to results which can be obtained using the former proposed indicators NO_y [*Milford et al.*, 1994], O_3/NO_z (with $NO_z = NO_y - NO_x$) and H_2O_2/HNO_3 [*Sillman*, 1995]. The aim of this comparison is not to define new threshold values for these indicators but to investigate the robustness of these indicators to the same parameters as investigated for Θ before. Realistic threshold values are difficult to investigate in box model studies if

deposition is an important loss reaction for the indicator species like it is here for HNO_3. The afternoon values of the NO_y compounds also depend on the initial NO_y concentration in the morning which was set to 0 in these box model runs but may be different in real cases.

For comparing the values from this study to those from studies of Milford and Sillman, it is important to notice that the definitions of the regimes are different. Milford and Sillman distinguished only between two regimes (NO_x-limited and VOC-limited), classifying parts of regime II to the NO_x regime and other parts to the VOC regime depending on whether the system is more sensitive to NO_x or VOC. With two regimes one can easily decide whether the reduction of VOC or of NO_x is more efficient for ozone abatement. However, it has the disadvantage that from this classification it is not possible to decide whether a reduction, for example, of VOC in a NO_x regime will provide reduced ozone values or not.

Milford et al. [1994] found from a numerical study over four cities and regions in the United States that afternoon NO_y values of less than 12 ppb were associated with ozone formation which is more sensitive to NO_x. Values over 25 ppb were associated with ozone formation more sensitive to VOC. NO_y mainly results from the reactions

$$\text{(R11)} \qquad OH + NO_2 \rightarrow HNO_3$$

$$\text{(R2), (R12)} \qquad RO_2 + NO \rightarrow (1 - \gamma)(RO + NO_2) + \gamma RONO_2.$$

While (R11) is a typical reaction for a NO_x-saturated system, the branching ratio γ from (R12) does not depend on the regime but only on the structure of RO_2. Especially in the case of a high ozone mixing ratio causing a high NO_2/NO ratio, PAN also becomes an important NO_y reservoir. Under those conditions, PAN and other acyl peroxy nitrates can reach high concentrations because after their thermal decomposition

$$\text{(-R14)} \qquad ROONO_2 \rightarrow RO_2 + NO_2,$$

most of the RO_2 radicals react again with NO_2:

$$\text{(R14)} \qquad RO_2 + NO_2 \rightarrow ROONO_2$$

and only a small amount undergoes loss reactions such as

$$\text{(R2)} \qquad RO_2 + NO \rightarrow (HO_2 \text{ or } RO_2) + NO_2 + \text{oxidized VOC}.$$

Similar to (R11), (R14) removes (at least temporarily) odd H from the cycle. An important difference to (R11) is the fact that the odd H loss reaction (R11) competes with the reaction VOC + OH which propagates the odd H cycle, whereas the low NO_x regime reactions of RO_2 with HO_2 or other peroxy radicals which compete with (R14) remove odd H like (R14). Therefore increased PAN formation does not influence the system in a way specific for high-NO_x regimes. *Tonnesen and Dennis* [2000a] found that the ratio of $[O_3]/[PAN]$ is not correlated to the border between regime I and regime II.

Further, the concentrations of organic nitrates and PAN are not only influenced by the relationship of the concentrations of different compounds but also by the absolute amount of reacting species. Thus in a highly polluted area with very high VOC concentrations and low NO_x/VOC ratios, high amounts of NO_y can be produced even if the regime is not regime I. Figure 5a shows that the isolines of the indicator NO_y are not at all parallel to the regime border but cross that line. The situation is the worst for the highest ozone concentrations. Here the high stability of PAN makes PAN the most important NO_y species. As explained before, the influence of the PAN production is not specific for the regime, but also for more usual ozone concentrations the isolines of NO_y cross the regime borders. Nevertheless, the indicator NO_y often provides good results in real cases. This may be due to the fact that the most common combinations of NO_x and VOC concentrations are only one segment of the whole set of theoretically possible combinations studied in this box model runs. This fact is illustrated by marking in Figure 5a usual NO_x and VOC concentrations for remote, rural, moderately polluted, and heavily polluted areas as given by *Finlayson-Pitts and Pitts* [1986]. If an indicator provides an isoline that divides this segment of common combinations correctly into an NO_x- and a VOC-sensitive part, it will provide good results in most of the cases. In the case of NO_y the isolines 20 and 40 cut the segment more or less into the same parts as the border between regime I and regime II. Hence, if the combination of NO_x and VOC concentrations is not different from usual values, the indicator values found by *Milford et al.* [1994] are in reasonable agreement to the results of this study. However, the results of this study suggest that the indicator NO_y may fail for other combinations of NO_x and VOC. Also, changes in the VOC split lowering or increasing the VOC reactivity or the nitrate formation yields influence NO_y significantly (see Table 2).

Because an increase of NO_x leads to lower O_3 and higher NO_y concentrations in regime I, ratios like O_3/NO_y or O_3/NO_z ($NO_z = NO_y - NO_x$) [*Sillman*, 1995; *Sillman et al.*, 1997] can be expected to improve the ability to distinguish between regimes I and II. However, Figure 5b shows no real improvement compared to the indicator NO_y, and Table 2 again provides a large overlap between the highest value found for regime I and the lowest found for regime II.

The indicator H_2O_2/HNO_3 [*Sillman*, 1995] which is strongly correlated to the ratio C_{VOC}/C_{NO_x} [*Stockwell*, 1986] mainly depends on the two reactions

$$\text{(R8)} \qquad 2\,HO_2 \rightarrow H_2O_2 + O_2$$

$$\text{(R11)} \qquad OH + NO_2[+M] \rightarrow HNO_3[+M].$$

The H_2O_2 formation is favored under conditions of NO_x control, and the HNO_3 formation is favored under conditions of NO_x saturation. For being a ratio of two typical reaction products this indicator shifts only slightly by increasing or lowering the absolute amount of reacting species in contrast to the behavior of indicators like NO_y and O_3/NO_z (see Figure 5c and Table 2). For the border between regime I and regime II, a value of 0.06 for the indicator H_2O_2/HNO_3 is deduced from the box model results. The sensitivity to other parameters is very similar to that of Θ. The largest exceeding values with respect to the threshold value of 0.06 for regime I are found for low temperatures and low reactivity. In the case of increased reactivity the behavior for the indicator H_2O_2/HNO_3 is somewhat more stable than that of Θ. As for Θ, the largest deviations for the indicator H_2O_2/HNO_3 from the values normally found for regime I and regime II are found in the case of artificially high nitrate formation rates. The values for determining the border between regime II and regime III show a significantly larger overlap and larger sensitivities than Θ. The value of 0.06 for the border between regimes I and II and a value ≥ 1 for the border between regime II and regime III are

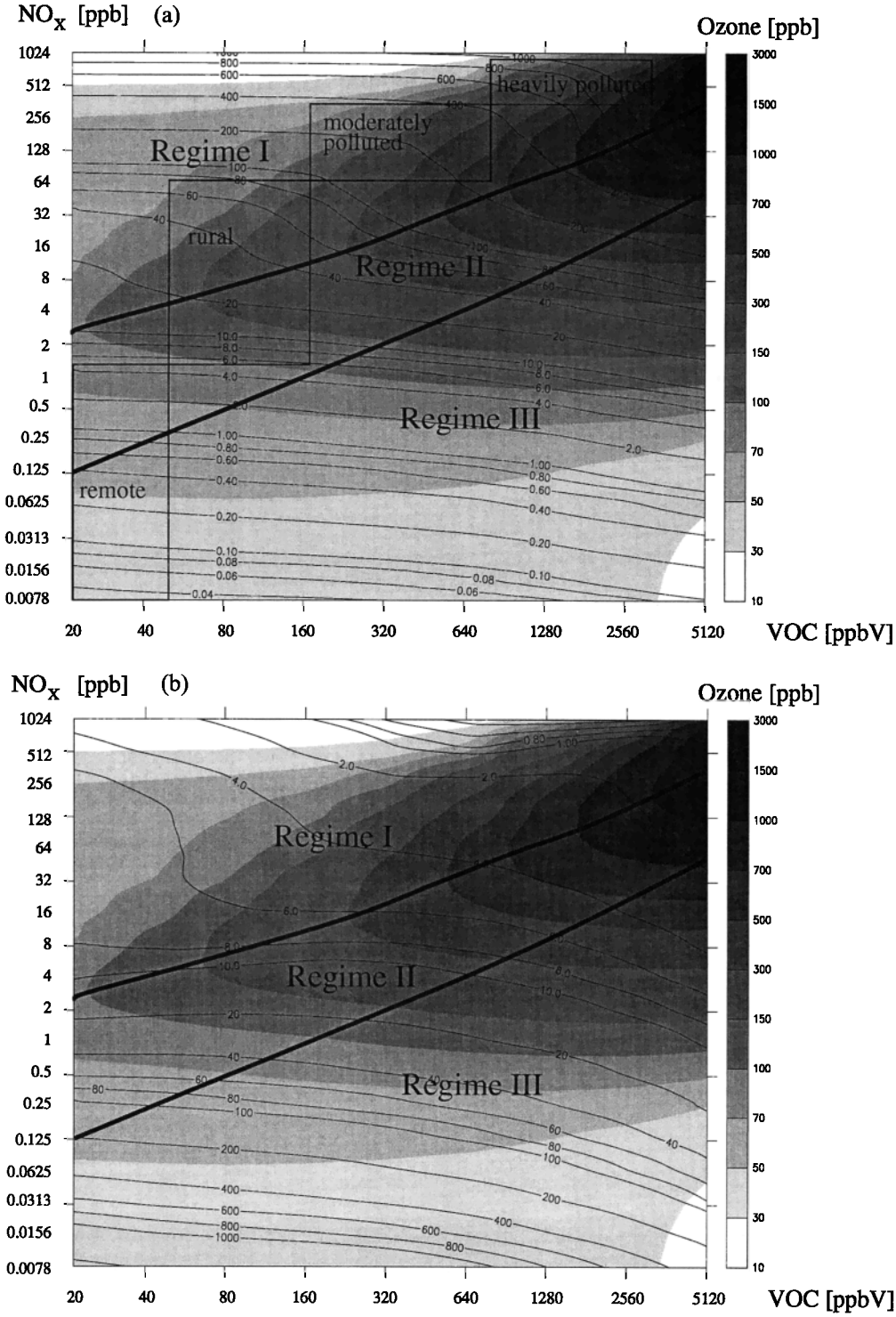

Figure 5. The three regimes of ozone formation and the indicator values of (a) NO_y, (b) O_3/NO_z, and (c) H_2O_2/HNO_3 calculated from the box model runs of the base case N4 (thin lines). The bold lines are the borders of the three regimes.

in agreement with the value of 0.4 suggested by *Sillman* [1995] for the border between a regime more sensitive to VOC and one more sensitive to NO_x.

Tonnesen and Dennis [2000a] published that for $P(H_2O_2)/P(HNO_3)$ the ratio of the production of H_2O_2 and HNO_3, a value of 0.06 to 0.07, is strongly associated with the ridgeline of O_x production, where O_x was defined as the sum of species that act as reservoirs of monatomic oxygen ($O_3 + O(^3P) + O(^1D) + NO_2 + 2\,NO_3 + 3\,N_2O_5 + PAN + RNO_3 + HNO_3$). Values between 0.12 and 0.2 for H_2O_2/HNO_3 were found to be associated with the border between regime I and regime II [*Tonnesen and Dennis*, 2000b].

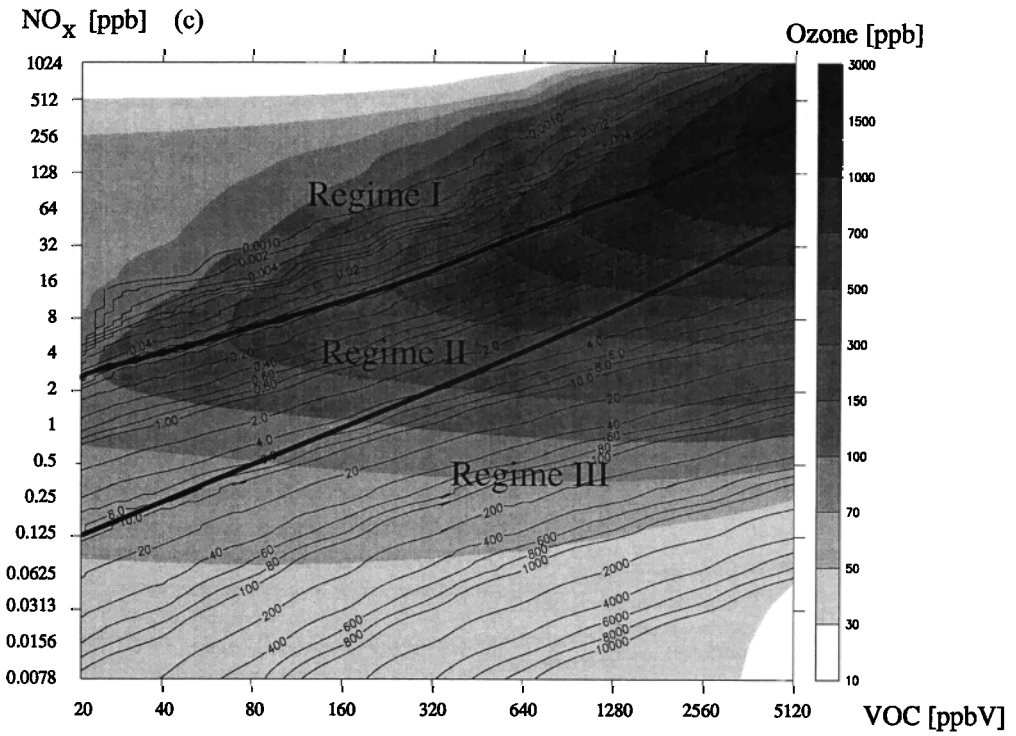

Figure 5. (continued)

5. 3-D Model Calculations

Three-dimensional studies were performed to test the behavior of the indicator Θ under conditions of variable emissions, transport, and dilution. Two questions should be answered by these simulations: (1) Is the indicator under these conditions still able to distinguish between the different regimes? (2) Can it be used to develop abatement strategies?

Three-dimensional model calculations were performed in two very different environments: in the highly polluted area of Athens and on the less polluted Swiss Plateau. The studies were aimed at testing the potential of the indicator (1) to distinguish between NO_x-limited and not NO_x-limited areas (that means to identify selectively regime I) and (2) to estimate the sensitivity of the ozone production due to changes in the VOC emissions (that means to distinguish between regimes II and III).

We tested the indicator by comparing its values to the change in the ozone concentrations due to additional emissions of NO_x or VOC. For ozone abatement strategies one will be more interested in the effectiveness of emission reductions than in the results of increasing the emissions. For an optimum test of the robustness of the indicator an emission increase is more suitable because it is possible to increase the emissions at all locations by the same amount. On the contrary, in the case of a reduction of the emissions one would be restricted by the fact that very low emissions occurring at some locations of the modeling areas cannot be further lowered.

5.1. Athens

In the 72 × 72 km modeling area of Athens the urban agglomeration of Athens is located in the center and has an extension of about 15 × 15 km. The surrounding area includes sea, rural, and mountain regions. The model runs were performed using a 2 × 2 km grid resolution and the model TVM [*Schayes et al.*, 1996; *Thunis*, 1995] with the chemical mechanism RACM. The simulations were done for September 14, 1994, a day when many trace gas measurements were performed in the greater Athens area during the MEDCAPHOT-TRACE campaign [*Fiorani et al.*, 1997; *Ziomas*, 1998]. September 14, 1994, was characterized by low-pressure gradients and clear-sky conditions [*Ziomas et al.*, 1998]. During the morning hours, weak northerly winds dominated, which transported the pollutants from the city over the sea. During the day a thermally induced sea breeze developed which transported photochemically active air masses back to the land. The highest ozone values are found in the early afternoon at 1400 and 1500 LT. The base case was simulated using the inventoried emissions, and the simulation results were in good agreement with field measurements [*Clappier et al.*, 1997, 1999].

5.1.1. Test case 1: Added NO_x emissions. In test case 1 the emissions of NO_x (90% NO and 10% NO_2) were increased between 0800 and 0900 LT over the whole area by 6 mol km^{-2} in the surface grid cells only. The original NO_x emissions varied at that time between 0 and 1600 mol km^{-2} h^{-1} with a mean value of 40. Together with the additional NO_x in each surface grid cell, either tracer A or tracer B was emitted, depending on the value of the indicator $\Theta = \tau_{OH}^{VOC}/\tau_{OH}^{NO_x}$ at 0800 LT in that grid cell. Tracer A was emitted from those grid cells where Θ was below 0.2, and tracer B was emitted from the other grid cells, with both tracers being defined as chemically inert. The emission rate was 6 mol km^{-2} h^{-1} and therefore identical with the one of the additional emitted NO_x. During the following hours of the simulation, this tracer study provided two important sources of information in the surface layer of the model: (1) Tracer A and tracer B provided information on the origin of the air parcel. (2) The sum of tracers A and B provided information on the amount of NO_x that was additionally emitted to this air parcel.

To account for the amount of tracers in the different grid cells of the surface layer, a value $V_{tr,x,y}$ is defined as

$$V_{tr,x,y} = \frac{C_{tr,x,y}}{\sum_{k=1}^{T}\left(\sum_{i=1}^{X}\left(\sum_{j=1}^{Y}(C_{k,i,j})\right)\right)/N} \quad (2)$$

where $C_{tr,x,y}$ is the concentration of the tracer tr (tr is tracer A or tracer B) in the surface grid cell xy, T is the number of different tracer species ($T = 2$ in this case), i and j are the coordinates in x and y direction, X and Y are the total number of surface grid cells in x and y direction, respectively, and N is the total number of grid cells in the surface layer of the model. Immediately after starting the release of the tracers, V_{tr} in each surface grid cell is 1 for the tracer that is emitted in this grid cell and 0 for the other tracer. Dilution occurs by vertical mixing and by transport across the borders of the modeling area. Later in the day, because V_{tr} is a relative value, the sum of V_A and V_B is greater than 1 for grid cells where the air is less diluted than the average and below 1 for dilution above the average. Surface grid cells with $\Sigma(V_{tr}) < 0.5$ were not considered because their air parcels were too far from the locations of NO_x emissions at 0800 LT, either at higher altitude or outside the modeling area. At noon the ozone concentrations in test case 1 at the ground level of the modeling area differ between −4 and +9 ppb from those of the base case result. At 1500 LT (the time of the highest daily ozone concentrations) the changes in ozone are in the range between −2 and +3 ppb. The grid cells of the surface layer were classified by their amount of ozone change. Table 3 and Figure 6 show these classes. Only those grid cells with $\Sigma(V_{tr}) \geq 0.5$ were considered. Table 3 shows for each class the number of cells, the number of considered cells ($\Sigma(V_{tr}) \geq 0.5$), and the average mixing ratio of tracers (corresponding to the additional NO_x) in the considered grid cells. Grid cells with only minor changes in the ozone mixing ratios show the highest dilution (highest number of not considered cells and smallest amount of total tracer). They correspond to the cells with smallest amount of additional NO_x.

The color bars in Figure 6 denote the partitioning of the two tracers within each class of cells. At noon those cells with ozone decrease contain high amounts of the tracer B and therefore originate from grid cells for which the indicator Θ indicates NO_x saturation at 0800 LT. In contrast, the air parcels with the largest ozone increases contain nearly no tracer B but high amounts of A. In the following hours, transport and mixing lower the contrast between the different air parcels, but nevertheless also at 1500 LT (the time of the highest daily ozone concentrations) the grid cells with ozone decrease contain about 80% of tracer B, whereas the grid cells with an increase of more than 2 ppb of ozone contain nearly 80% of tracer A.

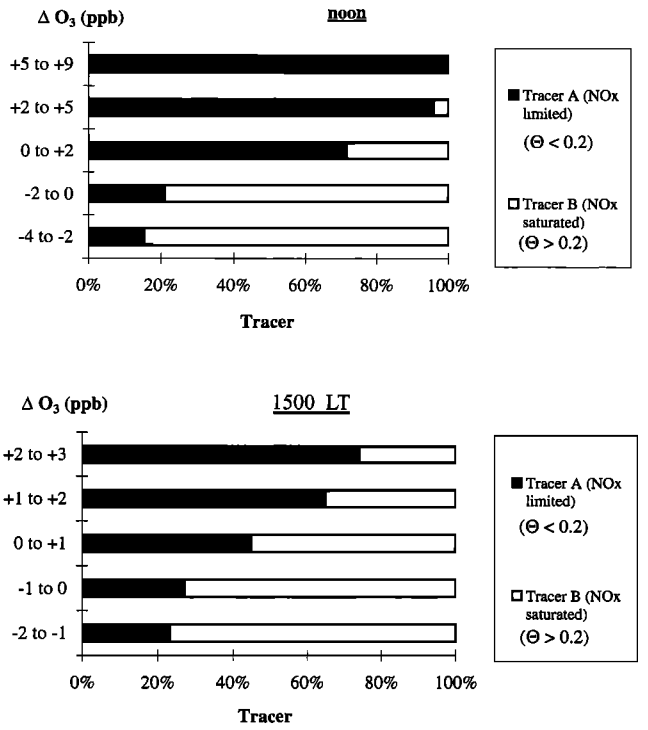

Figure 6. Comparison of the tracer concentrations and the changes in the ozone formation at noon and 1500 LT due to additional NO_x emissions in test case 1 (Athens). Only grid cells with $\Sigma V_{tr} \geq 0.5$ are considered.

Table 3. Test Case 1: Increased NO_x Emissions in Athens

Changes in the Ozone Mixing Ratios, ppb	Number of Grid Cells	Number of Grid Cells Considered	Mean Tracer Mixing Ratios, ppb
	Time: Noon		
−4 to −2	101	101	2.15
−2 to 0	728	478	1.17
0 to +2	415	54	0.99
+2 to +5	43	41	0.94
+5 to +9	9	9	1.79
	Time: 1500 LT		
−2 to −1	22	22	0.80
−1 to 0	147	103	0.32
0 to +1	1003	411	0.18
+1 to +2	110	110	0.25
+2 to +3	14	14	0.30

Figure 7 shows the noon and afternoon values of the indicators H_2O_2/HNO_3 and O_3/NO_z found in the grid cells with $\Sigma(V_{tr}) \geq 0.5$ and classified according to the changes in the ozone concentrations. The calculations were done estimating a concentration of 0 as initial value for all NO_z species. The threshold value of 0.06 found for the indicator H_2O_2/HNO_3 in the box model studies is reproduced by this 3-D study: At 1500 LT all grid cells where ozone values are increased by at least 1 ppb, compared to the base case, have indicator values higher than 0.06. All grid cells with ozone values decreased by at least 1 ppb have indicator values lower than 0.06. The noon and afternoon values of O_3/NO_z also show a good correlation to the ozone changes suggesting a threshold value somewhere between 10 and 14. Both of these threshold values may shift if the initial NO_z concentration is different from 0.

5.1.2. Test case 2: Added VOC emissions. Between 0800 and 0900 LT the mean value of VOC emissions over the whole modeling domain was 60 mol km^{-2}. For test case 2 the same amount of 60 mol km^{-2} VOC emissions was additionally emitted between 0800 and 0900 LT from each surface grid cell. At the same time, four tracers were emitted according to the values of Θ at 0800 LT at each grid cell: tracer E for $\Theta < 0.01$, tracer F for $0.01 < \Theta < 0.033$, tracer G for $0.033 < \Theta < 0.1$,

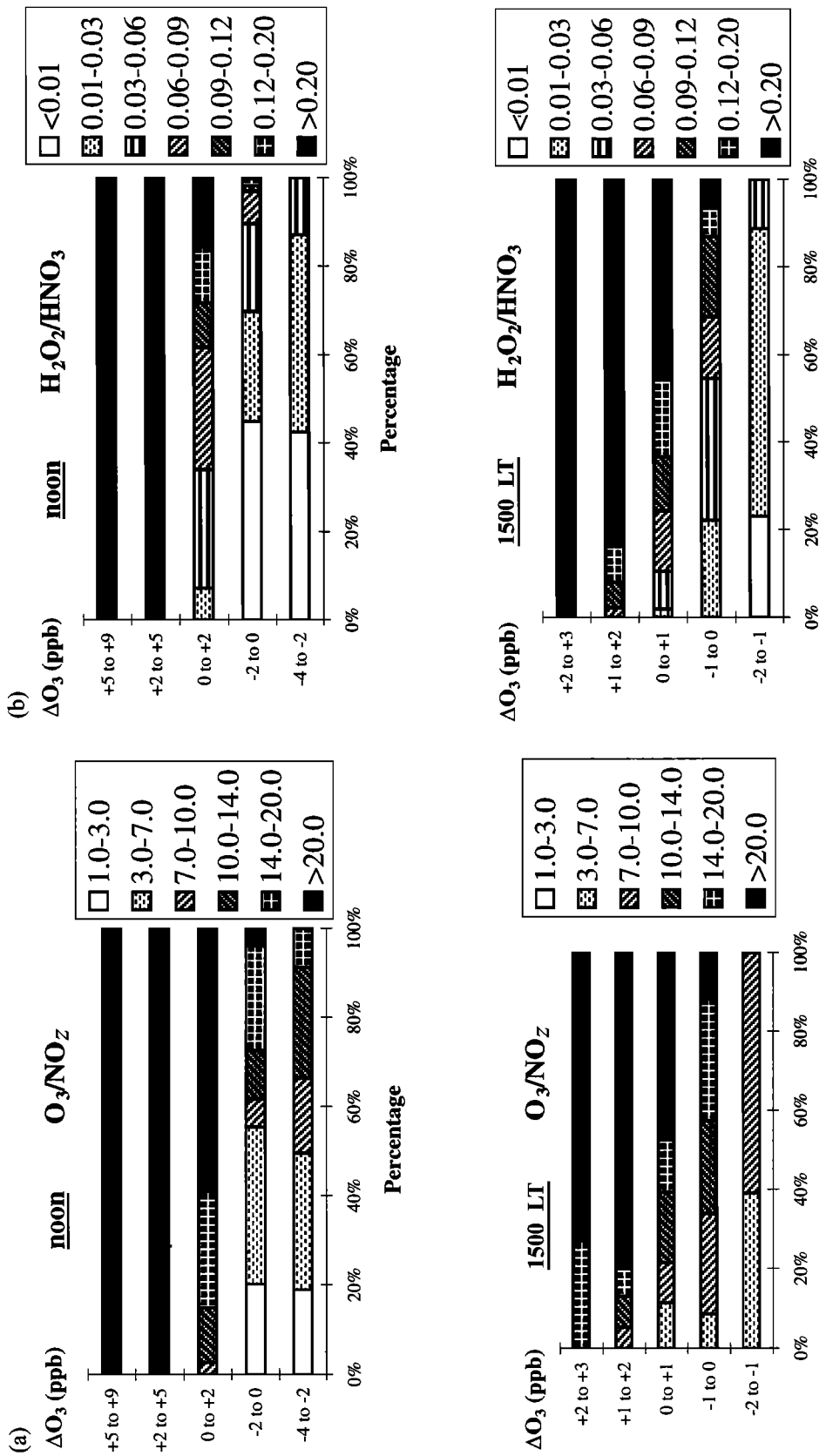

Figure 7. Comparison of the values of the indicators (a) O_3/NO_z and (b) H_2O_2/HNO_3 at noon and 1500 LT and the changes in the ozone formation due to additional NO_x emissions in the morning in the Athens area. Only grid cells with $\Sigma V_{rr} \geq 0.5$ are considered.

and tracer H for $\Theta > 0.1$. The emission rate of the tracers was the same as for the sum of the additional emitted VOC.

As in test case 1, the grid cells of the surface layer were classified by their amount of ozone change. Table 4 and Figure 8 show these classes. Here again, surface grid cells with $\Sigma(V_{tr}) < 0.5$ were not considered for the evaluation because their air parcels were too far from the locations of the additional VOC emissions at 0800 LT. Table 4 shows for each class the number of cells, the number of considered cells ($\Sigma(V_{tr}) \geq 0.5$), and the average mixing ratio of tracers (corresponding to the additional VOC) in the considered grid cells. As shown in Figure 8 at noon, small amounts of tracer H ($\Theta > 0.1$) are found in grid cells with lowered ozone mixing ratios, whereas percentages of more than 70% of tracer H are found in all grid cells in which the ozone mixing ratios increase by more than 2 ppb. On the other hand, tracer E (corresponding to morning values of $\Theta < 0.01$) is the prevailing tracer in the grid cells with lowered ozone, and only very small amounts of tracer E are found in grid cells with an ozone increase of more than 2 ppb. In the following hours, transport and mixing lower the contrast between the different air parcels. Nevertheless, at 1500 LT, the surface grid cells with ozone decrease contain about two thirds of tracer E, whereas the grid cells with an ozone increase contain about two thirds of tracer H with the highest percentages of H in the grid cells with largest ozone increase.

5.2. Swiss Plateau

The 180 × 380 km modeling area includes most of the Swiss Plateau and some small parts of Germany, Austria, France, and Italy. The largest city with about 1 million inhabitants, Zuerich, is located in the center of the modeling area. The model region includes remote, rural, and urban areas. The model runs were performed using a 5 × 5 km horizontal grid resolution and the model METPHOMOD [*Perego*, 1999] with the chemical mechanism RACM. As the base case, July 29, 1993, was simulated using the inventoried emissions. On that day the synoptic weather in Switzerland was dominated by westerly winds (average wind speed of about 7 m s^{-1}) which brought relatively clean air masses from the Atlantic Ocean into the modeling domain. Modeling results and field measurements were in good agreement [*Perego*, 1999; *Junier*, 1998].

5.2.1. Test case 3: Added NO_x emissions. Between 0800 and 0900 LT the mean value of NO_x emissions over the whole model domain was 6 mol km^{-2}. For the test case in the first 2 min after 0800 LT, the same amount of 6 mol km^{-2} NO_x emissions was additionally emitted from each surface grid cell. At the same time, two tracers are emitted according to the values of Θ at 0800 LT at each grid cell: tracer A for $\Theta < 0.2$ and tracer B for $\Theta > 0.2$. The emission rate of the tracers was the same as for the sum of the additional emitted NO_x.

As in the Athens case, the grid cells of the surface layer were classified by their amount of ozone change. Table 5 and Figure 9 show these classes. Here as well, the surface grid cells with $\Sigma(V_{tr}) < 0.5$ were not considered. Table 5 shows for each

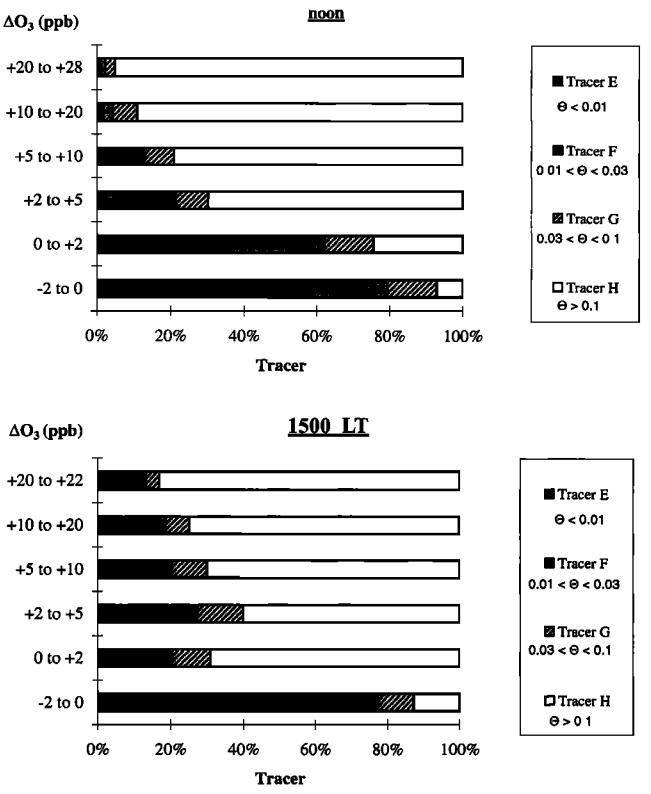

Figure 8. Comparison of the tracer concentrations and the changes in the ozone formation at noon and 1500 LT due to additional VOC emissions in the morning in test case 2 (Athens). Only grid cells with $\Sigma V_{tr} \geq 0.5$ are considered.

Table 4. Test Case 2: Increased VOC Emissions in Athens

Changes in the Ozone Mixing Ratios, ppb	Number of Grid Cells	Number of Grid Cells Considered	Mean Tracer Mixing Ratios, ppb
	Time: Noon		
−2 to 0	210	35	10.5
0 to +2	295	25	7.7
+2 to +5	237	123	5.6
+5 to +10	252	252	9.9
+10 to +20	253	253	16.5
+20 to +28	49	49	23.6
	Time: 1500 LT		
−1 to 0	312	66	1.16
0 to +2	704	365	1.42
+2 to +5	192	192	2.70
+5 to +10	52	52	4.21
+10 to +20	30	30	7.57
+20 to +22	6	6	9.22

Table 5. Test Case 3: Increased NO_x Emissions on the Swiss Plateau

Changes in the Ozone Mixing Ratios, ppb	Number of Grid Cells	Number of Grid Cells Considered	Mean Tracer Mixing Ratios, ppb
	Time: Noon		
−4 to −1	141	140	1.00
−1 to 0	720	511	0.47
0 to +2	1780	678	0.27
+2 to +5	400	375	0.32
+5 to +8	9	9	1.28
	Time: 1500 LT		
−1.2 to 0	372	61	0.21
0 to +2	2303	1470	0.14
+2 to +5	479	478	0.17
+5 to +10.5	3	3	1.13

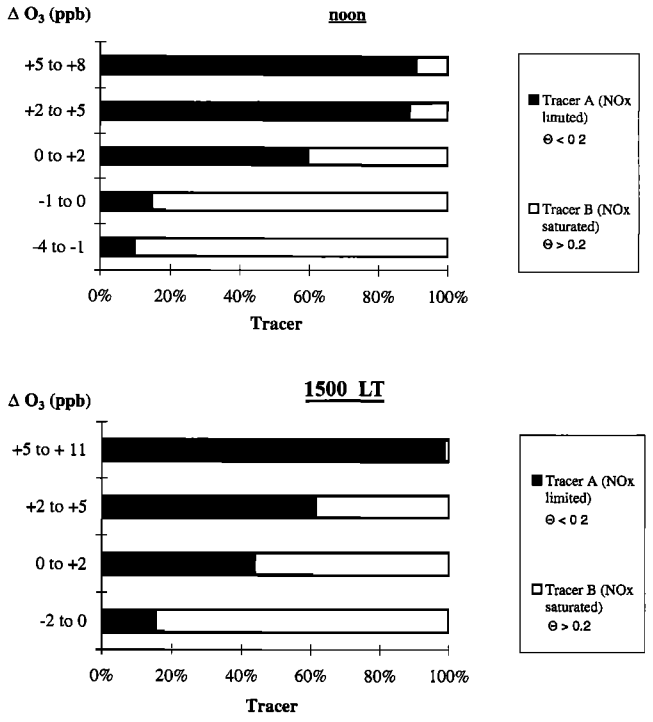

Figure 9. Comparison of the tracer concentrations and the changes in the ozone formation at noon and 1500 LT due to additional NO_x emissions in the morning in test case 3 (Swiss Plateau). Only grid cells with $\Sigma V_{tr} \geq 0.5$ are considered.

class the number of cells, the number of considered cells ($\Sigma(V_{tr}) \geq 0.5$), and the average mixing ratio of tracers (corresponding to the additional NO_x) in the considered grid cells. At noon, ozone reductions of up to 3.5 ppb and ozone increases of up to 8 ppb result from the additional emitted NO_x. Grid cells with ozone reduction contain more than 85% tracer B (which represents NO_x saturation at 0800 LT), whereas grid cells with ozone increases of more than 2 ppb contain more than 85% tracer A (which represents NO_x limitation at 0800 LT). At 1500 LT, grid cells with decreased ozone contain still more than 80% tracer B, and grid cells with an ozone increase of more than 5 ppb contain nearly only tracer A. For grid cells with an ozone increase between 2 and 5 ppb the percentage of tracer B is considerably increased compared to noon.

Table 6. Test Case 4: Increased VOC Emissions on the Swiss Plateau

Changes in the Ozone Mixing Ratios, ppb	Number of Grid Cells	Number of Grid Cells Considered	Mean Tracer Mixing Ratios, ppb
	Time: Noon		
Less than 0	830	148	0.47
0 to +1	1536	904	0.57
+1 to +2	264	264	1.15
+2 to +4	101	101	2.00
More than 4	5	5	3.34
	Time: 1500 LT		
Less than 0	969	344	0.19
0 to +1	1727	1205	0.27
+1 to +2	38	38	0.55
+2 to +4	2	2	1.12

5.2.2. Test case 4: Added VOC emissions. Between 0800 and 0900 LT the mean value of VOC emissions over the whole modeling domain was 10 mol km^{-2}. For the test case in the first 2 min after 0800 LT, the same amount of 10 mol km^{-2} VOC emissions was additionally emitted from each grid cell leading to an increase of the VOC mixing ratios in the lowest layer of about 2–3 ppbv. At the same time, four tracers were emitted according to the values of Θ at 0800 LT at each grid cell: tracer E for $\Theta < 0.01$, tracer F for $0.01 < \Theta < 0.033$, tracer G for $0.033 < \Theta < 0.1$, and tracer H for $\Theta > 0.1$. The emission rate of the tracers was the same as for the sum of the additional emitted VOC.

As in the Athens case, the grid cells of the surface layer were classified by their amount of ozone change. Table 6 and Figure 10 show these classes, without considering the surface grid cells with $\Sigma(V_{tr}) < 0.5$. Table 6 shows for each class the number of cells, the number of considered cells ($\Sigma(V_{tr}) \geq 0.5$), and the average mixing ratio of tracers (corresponding to the additional VOC) in the considered grid cells. As shown in Figure 10, the changes in the ozone values due to the additional VOC are much less pronounced than in the Athens case. At noon the largest ozone decrease is 0.6 ppb, and the largest increase is 5 ppb. At 1500 LT the changes are between −1 and +3 ppb ozone. Considerable amounts of tracers E (corresponding to morning values of $\Theta < 0.01$) are only found in areas with slightly decreased ozone, whereas increasing percentages of tracer H ($\Theta > 0.1$) are associated with enhanced ozone increase.

6. Discussion

The box model study shows that the new indicator $\Theta = \tau_{OH}^{VOC}/\tau_{OH}^{NO_x}$ is robust against most parameters besides the re-

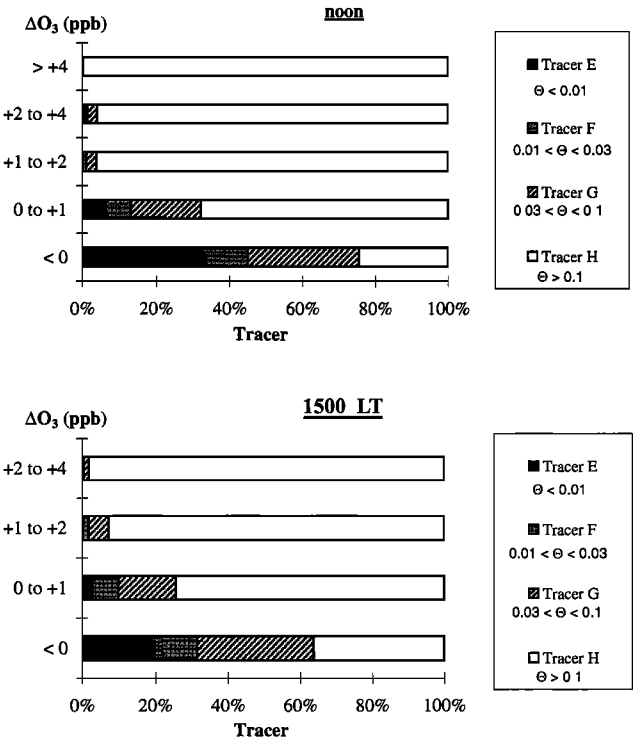

Figure 10. Comparison of the tracer concentrations and the changes in the ozone formation at noon and 1500 LT due to additional VOC emissions in the morning in test case 4 (Swiss Plateau). Only grid cells with $\Sigma V_{tr} \geq 0.5$ are considered.

gime. It is more robust than the indicators NO_y and O_3/NO_z and of comparable robustness as the indicator H_2O_2/HNO_3. Only very high nitrate production rates influence Θ severely. The amount of nitrate formation is the highest for large alkanes which are mainly emitted from diesel motors. Because the burning of diesel fuel also produces smaller alkanes and because its use is normally accompanied by gasoline consumption where the amount of emitted large alkanes is much smaller than from diesel fuel, that extreme case calculated in H1 and H2 will not exist in the real atmosphere. Therefore the real shift of Θ due to nitrate formation is much smaller than in these box model cases. Note that there is no significant difference between the Θ values obtained using the normal VOC split (N1–N6) and using the VOC split with strongly decreased nitrate formation (L1 and L2).

The 3-D simulations with increased NO_x emissions for Athens and the Swiss Plateau confirm the findings of the box model runs. The threshold value between regimes I and II is about 0.2. This shows that even if transport and dilution effects are taken into consideration, there is a strong correlation between the indicator value of an air parcel in the morning and the impact of changed morning NO_x emissions on the afternoon ozone concentrations. Thus measuring Θ values will give important information concerning at which locations additional NO_x emissions would have the lowest adverse impact on the air quality or at which place NO_x reduction would be most effective. This information cannot be directly provided by the earlier proposed indicators. Nevertheless, especially the indicator H_2O_2/HNO_3 provides also good results in this study, and the application of Θ in combination with an integrating indicator like H_2O_2/HNO_3 may lead to a very comprehensive understanding of the ozone formation at a given place.

The 3-D simulation runs for the Swiss Plateau show that tracer H which represents morning Θ values >0.1 is mainly associated with surface grid cells with significantly increased ozone values. The tracer E representing morning Θ values <0.01 is mainly found in grid cells with small ozone reductions. According to the box model runs, indicator values >0.01 should be associated with increased ozone. Therefore the large amounts of tracers F and G (representing morning Θ values between 0.01 and 0.1) in surface grid cells with small ozone reductions on the Swiss Plateau seem to be a contradiction. However, with (1) and a ΔC_{VOC} which is equal to a tracer concentration of 3 ppb it can be estimated that for an indicator value of 0.01 only 0.15 ppb ozone should be additionally produced. To produce more than 1 ppb additional ozone, the indicator value or the added VOC emissions should be about 10 times higher. In the Athens case where more additional VOC was emitted, the percentages of tracers F and G were higher in surface grid cells with increased ozone and lower in the grid cells with lowered ozone values. Therefore there is no disagreement between the box model study and the 3-D simulation concerning the threshold value of Θ for distinguishing regimes II and III.

7. Conclusions

$\Theta = \tau_{OH}^{VOC}/\tau_{OH}^{NO_x}$ is proposed as a new indicator for distinguishing between NO_x- and VOC-controlled ozone production. This indicator can be obtained by a combination of standard methods and a new pump and probe method. In contrast to other earlier proposed indicators, Θ is not based on long-lived species and therefore allows finding the instantaneous regime of an air parcel. Compared to the indicator NO_y and O_3/NO_z, the new indicator is less sensitive to the investigated parameters (e.g., photolysis, VOC reactivity, etc.). Its robustness is comparable to that of the indicator H_2O_2/HNO_3; both indicators have the largest problems if the nitrate formation is drastically increased which can be caused by very high percentages of large alkanes in the emissions. Θ values larger than 0.2 are associated with NO_x saturation, whereas indicator values below 0.01 represent air masses nearly insensitive to VOC.

Three-dimensional simulations with additional NO_x emissions revealed that the morning values of Θ and the changes in the ozone concentrations several hours after measuring Θ and releasing the additional emission are highly correlated. Also, in the case of additional emitted VOC emissions there is a good correlation between Θ and the changes in the ozone. For the development of abatement strategies it is important that the value of the indicator Θ enables a forecast, in which way the ozone concentrations several hours later are influenced by increasing or decreasing the emissions.

Acknowledgments. The authors are grateful to the Swiss National Science Foundation (grant 21-50861.97) and the CTI SATURN project (3260.1) for supporting this work. The authors would like to thank each of the referees for their helpful comments and suggestions. The authors are also grateful to Ed Browell and his team at NASA Langley for stimulating discussions.

References

Calpini, B., F. Jeanneret, M. Bourqui, A. Clappier, R. Vajtai, and H. van den Bergh, Direct measurement of the total reaction rate of OH in the atmosphere, *Analusis*, *27*(4), 328–336, 1999.

Clappier, A., A. Martilli, B. Calpini, H. van den Bergh, and B. C. Kruger, Photochemical studies with the model CTC for the Athens 2004 project, in *Proceedings of the International Scientific Workshop "Athens 2004 Air Quality Study,"* edited by N. Moussiopoulos and S. Papagrigoriou, pp. 133–142, Athens 2004 Bid Comm., Athens, 1997.

Clappier, A., A. Martilli, P. Grossi, P. Thunis, F. Pasi, B. C. Krüger, B. Calpini, G. Graziani, and H. van den Bergh, Effect of sea breeze on the air pollution in the greater Athens area, part 1, Numerical simulations and field observations, *J. Appl. Meteorol.*, *39*, 563–575, 1999.

Finlayson-Pitts, B. J., and J. N. Pitts, *Atmospheric Chemistry: Fundamentals and Experimental Techniques*, Wiley-Interscience, New York, 1986.

Fiorani, L., B. Calpini, L. Jaquet, H. van den Bergh, and E. Durieux, A combined determination of wind velocities and ozone concentrations for a first measurement of ozone fluxes with a DIAL instrument during the MEDCAPHOT-TRACE campaign, *Atmos. Environ.*, *32*, 2151–2159, 1997.

Jeanneret, F., F. Kirchner, A. Clappier, H. van den Bergh, and B. Calpini, Total VOC reactivity in the planetary boundary layer, 1, Estimation by a pump and probe OH experiment, *J. Geophys. Res.*, this issue.

Junier, M., Etude de la pollution photochimique sur le Plateau suisse à l'aide d'un modèle eulérien tridimensionnel, diploma work, Swiss Fed. Inst. of Technol., Lausanne, Switzerland, 1998.

Kleinman, L. I., Photochemical formation of peroxides in the boundary layer, *J. Geophys. Res.*, *91*, 10,889–10,904, 1986.

Kleinman, L. I., Seasonal dependence of boundary layer peroxide concentration: The low- and high-NO_x regimes, *J. Geophys. Res.*, *96*, 20,721–20,734, 1991.

Kuhn, M., et al., Intercomparison of the gas-phase chemistry in several chemistry and transport models, *Atmos. Environ.*, *32*, 693–709, 1998.

Lu, C. H., and J. S. Chang, On the indicator-based approach to assess ozone sensitivities and emissions features, *J. Geophys. Res.*, *103*, 3453–3462, 1998.

Milford, J., D. Gao, S. Sillman, P. Blossey, and A. G. Russell, Total reactive nitrogen (NO_y) as an indicator for the sensitivity of ozone to NO_x and hydrocarbons, *J. Geophys. Res.*, *99*, 3533–3542, 1994.

Perego, S., Metphomod: A numerical mesoscale model for simulation of regional photosmog in complex terrain: Model description and

application during Pollumet 1993 (Switzerland), *Meteorol. Atmos. Phys.*, *70*, 43–69, 1999.

Schayes, G., P. Thunis, and R. Bornstein, Topographic vorticity-mode mesoscale-β (TVM) model, part I, Formulation, *J. Appl. Meteorol.*, *35*, 1815–1823, 1996.

Sillman, S., The use of NO_y, H_2O_2, and HNO_3 as indicators for ozone-NO_x-hydrocarbon sensitivity in urban locations, *J. Geophys. Res.*, *100*, 14,175–14,188, 1995.

Sillman, S., D. He, C. Cardelino, and R. E. Imhoff, The use of photochemical indicators to evaluate ozone-NO_x-hydrocarbon sensitivity: Case studies from Atlanta, New York, and Los Angeles, *J. Air Waste Manage. Assoc.*, *47*, 1030–1040, 1997.

Sillman, S., D. He, M. R. Pippin, P. H. Daum, D. G. Imre, L. I. Kleinman, J. H. Lee, and J. Weinstein-Lloyd, Model correlations for ozone, reactive nitrogen, and peroxides for Nashville in comparison with measurements: Implications for O_3-NO_x-hydrocarbon chemistry, *J. Geophys. Res.*, *103*, 22,629–22,644, 1998.

Stockwell, W. R., A homogeneous gas phase mechanism for use in a regional acid deposition model, *Atmos. Environ.*, *20*, 1615–1632, 1986.

Stockwell, W. R., P. Middleton, J. S. Chang, and X. Tang, The second generation regional acid deposition model: Chemical mechanism for regional air quality modeling, *J. Geophys. Res.*, *95*, 16,343–16,367, 1990.

Stockwell, W. R., F. Kirchner, M. Kuhn, and S. Seefeld, A new mechanism for regional atmospheric chemistry modeling, *J. Geophys. Res.*, *102*, 25,847–25,879, 1997.

Thunis, P., Formulation and evaluation of a nonhydrostatic vorticity-mode mesoscale model, *Rep. EUR16141EN*, Eur. Comm., Luxembourg, 1995.

Tonnesen, G. S., and R. L. Dennis, Analysis of radical propagation efficiency to assess ozone sensitivity to hydrocarbons and NO_x, 1, Local indicators of instantaneous odd oxygen production sensitivity, *J. Geophys. Res.*, *105*, 9213–9225, 2000a.

Tonnesen, G. S., and R. L. Dennis, Analysis of radical propagation efficiency to assess ozone sensitivity to hydrocarbons and NO_x, 2, Long-lived species as indicators of ozone concentration sensitivity, *J. Geophys. Res.*, *105*, 9227–9241, 2000b.

Ziomas, I., The Mediterranean campaign of photochemical tracers-transport and chemical evolution (MEDCAPHOT-TRACE): An outline, *Atmos. Environ.*, *32*, 2055–2069, 1998.

Ziomas, I., P. Tzoumaka, D. Balis, D. Melas, C. S. Zerefos, and O. Klemm, Ozone episodes in Athens, Greece: A modelling approach using data from the MEDCAPHOT-TRACE, *Atmos. Environ.*, *32*, 2313–2321, 1998.

B. Calpini (corresponding author), A. Clappier, F. Jeanneret, F. Kirchner, B. Krüger, and H. van den Bergh, Air Pollution Laboratory (LPA), Swiss Federal Institute of Technology (EPFL), 1015 Lausanne, Switzerland. (bertrand.calpini@epfl.ch)

(Received February 14, 2000; revised August 30, 2000;
accepted September 15, 2000.)